

Axion search via Coulomb-assisted quantum vacuum birefringence

Stefan Evans^{1,*} and Ralf Schützhold^{1,2}

¹*Helmholtz-Zentrum Dresden-Rossendorf, Bautzner Landstraße 400, 01328 Dresden, Germany*

²*Institut für Theoretische Physik, Technische Universität Dresden, 01062 Dresden, Germany*
(Dated: July 18, 2023)

We study the impact of axions or axion-like particles on birefringent (i.e., polarization changing) scattering of x-ray photons at the Coulomb field of nuclei superimposed by optical lasers of ultra-high intensity. Applying the specifications of the Helmholtz International Beamline for Extreme Fields (HIBEF), we find that this set-up can be more sensitive than previous experiments such as PVLAS in a large domain of parameter space. Furthermore, by changing the pump and probe laser orientations and frequencies, one can scan different axion masses.

Introduction After the discovery of the Higgs particle [1], axions or axion-like particles are one of the most favorite candidates for new physics beyond the standard model. One way to motivate them is to consider the electromagnetic field strength tensor $F_{\mu\nu}$ and its dual $\tilde{F}_{\mu\nu}$ which can be contracted to yield the two lowest-order Lorentz invariants $F_{\mu\nu}F^{\mu\nu} = 2(\mathbf{B}^2 - \mathbf{E}^2) = -\tilde{F}_{\mu\nu}\tilde{F}^{\mu\nu}$ as well as $\tilde{F}_{\mu\nu}F^{\mu\nu} = -4\mathbf{B} \cdot \mathbf{E}$. The former generates the Lagrangian density of electromagnetism while the latter is usually discarded because it is a total derivative. However, this argument is only valid if the pre-factor in front of this term $\tilde{F}_{\mu\nu}F^{\mu\nu}$ is a constant. If this pre-factor is a dynamical field ϕ , i.e., space-time dependent, this term does generate a non-trivial (effective) interaction Lagrangian of the form ($\hbar = c = 1$)

$$\mathcal{L}_{\text{int}} = g_\phi \phi \mathbf{B} \cdot \mathbf{E}, \quad (1)$$

where g_ϕ denotes the (effective) interaction strength. Since the term $\tilde{F}_{\mu\nu}F^{\mu\nu}$ is odd under parity \mathcal{P} , the axion field ϕ is usually considered a pseudoscalar field.

Apart from this effective field theory approach, axions were originally proposed as a possible solution to the strong \mathcal{CP} problem in quantum chromodynamics (QCD), see, e.g., [2–8]. In the following, axions and axion-like particles will be used synonymously. Modeling the axion field as a massive scalar field weakly coupled to the other standard model particles, it could also be a candidate for dark matter [9–18] and would have important consequences for cosmology, see, e.g., [19–26].

In search of observable effects, astronomical data provide very important sources [27]. Similar to neutrinos, weakly coupled and long lived axions could provide a cooling mechanism for stars and other astrophysical objects (such as white dwarfs [28]), mostly due to their coupling (1) to photons. In fact, the apparent absence of such effects for our sun, for example, leads to significant restrictions on the parameter space of axions [29].

Nevertheless, such astronomical observations cannot supersede laboratory experiments. On the one hand, a direct and active experimental manipulation is qualitatively different from an indirect observation, in particular since our conclusions drawn from the latter depend on

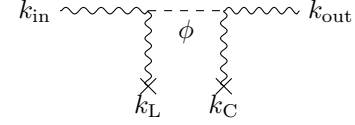


FIG. 1. Axion s -channel contribution to light-by-light scattering. The initial and final x-ray photons with momenta k_{in} and k_{out} interact with the field of the optical laser k_L and the nuclear Coulomb field k_C via the internal axion propagator (dashed line).

our correct understanding of stellar dynamics etc. On the other hand, there are many reasons why axions detected in the laboratory could still be consistent with astronomical observations (especially if they occur on very different scales) [30–37], for example interaction effects such as running coupling constants or axion confinement [38, 39].

Laboratory searches for axions include “light shining through wall” experiments [40–51] based on the creation of axions from electromagnetic fields via the coupling (1). Then, after propagating a macroscopic distance (through the wall), the axion is converted back into an electromagnetic signal. As a qualitatively different class of scenarios, effective photon-photon interactions (light-by-light scattering) could be mediated by an internal axion line [52–63], see also Fig. 1. In this case, the axion does not propagate a macroscopic distance and thus such experiments would also be sensitive to axions which are not quasi-free and long-lived (at the scales relevant to the experiment).

Prominent examples for the second class are PVLAS (“Polarizzazione del Vuoto con LASer”, i.e., polarization of the vacuum with a laser) [64–66], BMV [67, 68] and OVAL [69]. Using a strong and static magnetic field as the pump field for polarizing the vacuum, the goal was to detect this change with an optical laser as the probe field. The sought-after signal was then a rotation or flip of the optical laser polarization, i.e., quantum vacuum birefringence.

In this work, we study an alternative scenario which is motivated by a recent proposal [70] for detecting quantum vacuum birefringence as predicted by quantum electrodynamics (QED). As the probe field, we envision x-ray

photons generated by an x-ray free electron laser (XFEL) because their high frequency increases the signal. The pump field is supposed to be a superposition of an optical laser and the Coulomb field of a nucleus. Both offer pump field strengths much larger than in PVLAS, while the spatial inhomogeneity of the Coulomb field facilitates a finite scattering angle (in the mrad regime) which helps us to discriminate the signal photons from the background (the main XFEL beam).

Geometry To illustrate our main idea, let us start with the most simple set-up. The initial x-ray photon is described by its energy ω_{in} , momentum $\mathbf{k}_{\text{in}} = \omega_{\text{in}}\mathbf{n}_{\text{in}}$, polarization \mathbf{e}_{in} , and analogously for the final x-ray photon with ω_{out} , $\mathbf{k}_{\text{out}} = \omega_{\text{out}}\mathbf{n}_{\text{out}}$ and \mathbf{e}_{out} , as well as for the optical laser photon with ω_{L} , $\mathbf{k}_{\text{L}} = \omega_{\text{L}}\mathbf{n}_{\text{L}}$ and \mathbf{e}_{L} . Finally, the Coulomb field of the nucleus is represented by the wavenumber \mathbf{k}_{C} (and zero frequency).

In order to obtain a resonant enhancement of our signal (see below), we consider the case where the optical laser photon is absorbed (instead of emitted) such that energy and momentum conservation read

$$\omega_{\text{out}} = \omega_{\text{in}} + \omega_{\text{L}}, \quad \mathbf{k}_{\text{out}} = \mathbf{k}_{\text{in}} + \mathbf{k}_{\text{L}} + \mathbf{k}_{\text{C}}. \quad (2)$$

Since we consider the birefringent $\mathbf{e}_{\text{in}} \perp \mathbf{e}_{\text{out}}$ signal in or close to forward direction $\mathbf{n}_{\text{in}} \approx \mathbf{n}_{\text{out}}$, the direct interaction (1) between the initial and final x-ray photons is suppressed and hence we focus on the s -channel in Fig. 1 and neglect the t -channel (see below).

As a consequence, each vertex (1) combines an x-ray photon with either the optical laser or the Coulomb field. By adjusting the polarization and propagation unit vectors appropriately, we can select the various possibilities. For example, in the fully perpendicular case $\mathbf{n}_{\text{L}} \parallel \mathbf{e}_{\text{out}}$ and $\mathbf{e}_{\text{L}} \parallel \mathbf{n}_{\text{in}}$, the optical laser cannot couple to the final x-ray photon since their electric and magnetic fields are orthogonal to each other. Thus, the magnetic component of the optical laser can only couple to the electric component of the initial x-ray photon while the Coulomb field couples to the magnetic component of the final x-ray photon.

Axion Propagator The lowest-order Feynman diagram of the process under consideration is displayed in Fig. 1. In terms of the four vectors $\underline{k}_{\text{in}}$ and \underline{k}_{L} , the four-momentum of the internal axion line reads $\underline{p}_{\phi} = \underline{k}_{\text{in}} + \underline{k}_{\text{L}}$ and thus its contribution to the amplitude becomes

$$\frac{g_{\phi}^2}{(\underline{k}_{\text{in}} + \underline{k}_{\text{L}})^2 - m_{\phi}^2} = \frac{g_{\phi}^2}{\omega_{\text{in}}\omega_{\text{L}} - \mathbf{k}_{\text{in}} \cdot \mathbf{k}_{\text{L}} - m_{\phi}^2}, \quad (3)$$

where we have assumed that axion can be described by the standard propagator of a scalar field with mass m_{ϕ} .

For the geometry discussed above, we have $\mathbf{k}_{\text{in}} \perp \mathbf{k}_{\text{L}}$ and thus the amplitude would be enhanced strongly near the resonance $\omega_{\text{in}}\omega_{\text{L}} \approx m_{\phi}^2$ corresponding to an axion mass of order $\mathcal{O}(10^2 \text{ eV})$. By varying the angle between the optical laser and the XFEL, one can scan different axion masses (see below).

In fact, exactly on resonance $\omega_{\text{in}}\omega_{\text{L}} = m_{\phi}^2$, the amplitude would actually diverge in the case of perfect plane waves. Of course, this implies that higher orders in g_{ϕ} should be taken into account. A simple way of effectively doing this could be to include self-energy terms in the propagator containing an imaginary part which then corresponds to a decay rate $\Gamma_{\phi} \sim g_{\phi}^2$. In our case, this is not necessary since the optical laser is not a perfect plane wave, but a focused beam – with a finite momentum spread $\Delta\mathbf{k}_{\text{L}}$ which thus regularizes the amplitude (3).

Coulomb Field In the scenario considered above, the fourth external photon line represents the Coulomb field of the nucleus. Inserting the Fourier transform of the Coulomb field

$$\int d^3r e^{i\mathbf{k}_{\text{C}} \cdot \mathbf{r}} \frac{Q}{4\pi r^2} \mathbf{e}_r = iQ \frac{\mathbf{k}_{\text{C}}}{\mathbf{k}_{\text{C}}^2}, \quad (4)$$

we see that the $\mathbf{B} \cdot \mathbf{E}$ coupling (1) requires a component of \mathbf{k}_{C} parallel to the magnetic component of the outgoing x-ray photon in order to obtain a non-zero amplitude. In the fully perpendicular case $\mathbf{n}_{\text{L}} \parallel \mathbf{e}_{\text{out}}$ and $\mathbf{e}_{\text{L}} \parallel \mathbf{n}_{\text{in}}$ considered here, this implies that the final photons must be scattered out of the plane spanned by the two initial beams \mathbf{k}_{in} and \mathbf{k}_{L} .

As another important point, the $1/r^2$ scaling from the Coulomb field cancels the r^2 volume factor in the d^3r integration. As a consequence, the spatial integration is cut off by the momentum \mathbf{k}_{C} resulting in a potentially large interaction volume – which may even span many XFEL wavelengths. To exploit this large interaction volume, we consider cases where not just \mathbf{k}_{L} but also the momentum transfer $\mathbf{k}_{\text{out}} - \mathbf{k}_{\text{in}}$ and thus also \mathbf{k}_{C} are in the optical or near-optical regime, see below.

Amplitude Combining the results above, the amplitude for the process under consideration reads

$$\mathfrak{A}^s = g_{\phi}^2 \frac{\omega_{\text{in}}(\mathbf{e}_{\text{in}} \cdot [\mathbf{k}_{\text{L}} \times \mathbf{A}_{\text{L}}])([\mathbf{k}_{\text{out}} \times \mathbf{e}_{\text{out}}] \cdot \mathbf{k}_{\text{C}})}{\omega_{\text{in}}\omega_{\text{L}} - \mathbf{k}_{\text{in}} \cdot \mathbf{k}_{\text{L}} - m_{\phi}^2} \frac{Q}{\mathbf{k}_{\text{C}}^2}, \quad (5)$$

where \mathbf{A}_{L} denotes the vector potential of the optical laser. As explained above, the realistic description of a laser focus which is localized in space requires the average over a finite momentum spread $\int d^3k_{\text{L}}$, which we implement with a distribution function $\mathbf{A}_{\text{L}}(\mathbf{k}_{\text{L}})$. This averaging procedure then also regularizes the resonant singularity of the axion propagator at $\omega_{\text{in}}\omega_{\text{L}} - \mathbf{k}_{\text{in}} \cdot \mathbf{k}_{\text{L}} = m_{\phi}^2$.

A finite temporal duration of the optical laser pulse would correspond to a spread in its frequency $\omega_{\text{L}} = |\mathbf{k}_{\text{L}}|$ but we neglect this spread here and focus on a fixed frequency $\omega_{\text{L}} = |\mathbf{k}_{\text{L}}|$ for simplicity.

Experimental Parameters Taking the specifications of the Helmholtz International Beamline for Extreme Fields (HIBEF) as an example, we consider the following experimental setup, as illustrated in Fig. 2. The optical laser is characterized by its frequency $\omega_{\text{L}} = 1.5 \text{ eV}$, focus intensity $\mathbf{E}^2 = 4 \times 10^{21} \text{ W/cm}^2$, with a $3 \mu\text{m}$ waist and a divergence of ± 15 degrees. We model the optical laser focus by

a superposition of plane waves with the same frequency ω_L and a Gaussian distribution for the transversal momentum spread. Assuming a repetition rate of 5 Hz [71], one could carry out an experiment with $\mathcal{O}(10^3)$ shots in a matter of minutes, such that we set $\mathcal{O}(10^{-3})$ birefringent x-ray photons per shot as our detection threshold.

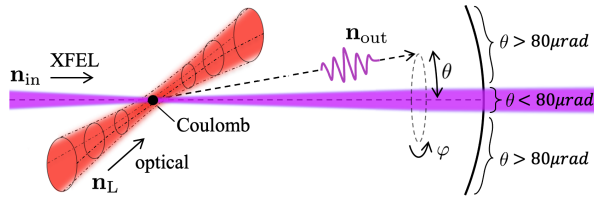


FIG. 2. Sketch of the experimental set-up.

For the Coulomb contribution to the pump field, we assume the same scenario as already studied in [70] where the optical laser (or a suitable pre-pulse) fully ionizes a 100 nm size carbon target and blows out almost all the electrons, leaving behind a cloud of $N_C = 10^8$ nuclei. As an important point, these nuclei are very close together (before the Coulomb explosion) such that the scattered x-rays with momentum transfer in the eV regime cannot resolve single nuclei and thus the amplitudes of all these nuclei add up coherently – resulting in an effective single giant nucleus with charge $N_C Q$.

We probe the Coulomb-assisted optical laser background using an XFEL pulse of frequency $\omega_{in} = 10$ keV, comprising $N_{XFEL} = 10^{12}$ photons per shot, with a beam waist of $5 \mu\text{m}$ and a $80 \mu\text{rad}$ beam divergence [71, 72]. The combined momentum transfer supplied by pump field, being in the near-optical regime, scatters the XFEL photons outside of this $80 \mu\text{rad}$ cone. Combining this consideration with the Coulomb target specifications above, we thus search for a signal between $80 \mu\text{rad} < \theta < 2$ mrad.

Axion Signal Now we are in the position to estimate the signal strength. As motivated above, we focus on the s -channel amplitude as the dominant contribution, the t -channel and the pure QED term are discussed in the Appendix. Although only the absorption case (2) yields a resonant enhancement and is thus the most important contribution, we also include the emission case for the sake of completeness and sum over both cases $\omega_{out} = \omega_{in} \pm \omega_L$. Furthermore, we sum the diagram in Fig. 1 and the reverse sequence (exchanging optical and Coulomb field interactions). Averaging the optical photons over the transverse momentum spread, we obtain the birefringent ($\mathbf{e}_{in} \perp \mathbf{e}_{out}$) differential cross section

$$\frac{d\sigma}{d\Omega} = \sum_{\pm} \frac{|\mathfrak{A}_{\pm}^s|^2}{4(2\pi)^2}, \quad (6)$$

where we have used that $\omega_{out}/\omega_{in} \approx 1$. Subscripts \pm label summation over both cases of absorbed and emitted optical photons $\omega_{out} = \omega_{in} \pm \omega_L$.

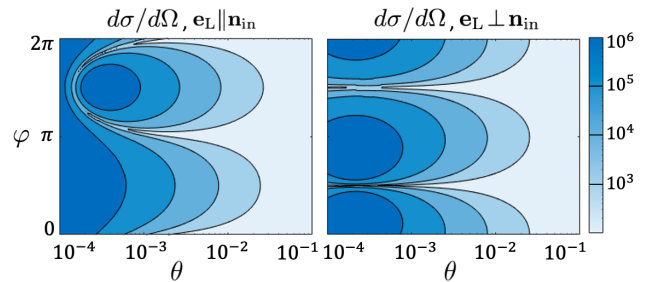


FIG. 3. Differential cross section $d\sigma/d\Omega$ according to Eq. (6) in units of 10^{-30} eV^{-2} for two geometries and $m_\phi = 180 \text{ eV}$ as well as $g_\phi = 10^{-2} \text{ GeV}^{-1}$.

To illustrate the impact of the geometry, we plot Eq. (6) in Fig. 3 in the range $80 \mu\text{rad} < \theta < 0.1 \text{ rad}$ and $0 < \varphi < 2\pi$ for two scenarios. In the left plot, we consider the fully perpendicular case, $\mathbf{n}_L \parallel \mathbf{e}_{out}$ and $\mathbf{e}_L \parallel \mathbf{n}_{in}$. As explained after Eq. (4), in this case scattering is dominant out of the plane spanned by \mathbf{n}_L and \mathbf{n}_{in} , i.e., for $\varphi = \pi/2$ or $3\pi/2$. In contrast, the right plot in Fig. 3 corresponds to the rotated laser polarization $\mathbf{e}_L \perp \mathbf{n}_{in}$. In this case, the electric component of the optical laser couples to the magnetic component of the x-ray at one vertex while the Coulomb field couples to the magnetic component of the x-ray at the other vertex. For a birefringent signal, these two directions must be perpendicular such that scattering is now dominant in the plane spanned by \mathbf{n}_L and \mathbf{n}_{in} , i.e., for $\varphi = 0$ or π . As discussed below, in order to suppress a possible background from the residual electrons, the first scenario (left plot in Fig. 3) might be advantageous in comparison to the second (right plot in Fig. 3).

To determine the total number N_{signal} of signal photons, we integrate (6) over the domain of scattering angles discussed above $80 \mu\text{rad} < \theta < 2$ mrad. Taking into account the XFEL photon number N_{XFEL} per shot multiplied by the number 10^3 of shots and the size of the XFEL focus $w_{XFEL} = 5 \mu\text{m}$, we find

$$N_{\text{signal}} \approx 10^3 \frac{N_{XFEL} N_C^2}{w_{XFEL}^2} \int_0^{2\pi} d\phi \int_{8 \cdot 10^{-5}}^{2 \cdot 10^{-3}} d\theta \sin \theta \frac{d\sigma}{d\Omega}, \quad (7)$$

where the factor N_C^2 arises from the coherent addition of the large number N_C of nuclei.

In Fig. 4 we plot the domain of accessible axion parameter space as the coupling g_ϕ and mass m_ϕ for which $N_{\text{signal}} \geq 1$ in (7), i.e., one or more signal photons per thousand XFEL shots. We display three optical laser orientations, the fully perpendicular case $\mathbf{k}_{in} \perp \mathbf{k}_L$ sketched in Fig. 2, here labeled $\vartheta = \pi/2$, as well as the cases $\vartheta = \pi/4$ and $\vartheta = 3\pi/4$, where ϑ denotes the angle between the optical laser and the XFEL.

As already discussed after Eq. (3), varying this angle effectively amounts to scanning different ranges of the axion mass. Indeed, when going from $\vartheta = \pi/4$ to $3\pi/4$,

the resonance shifts to higher axion masses and becomes more narrow. As a result, the enhancement of the signal at resonance increases. E.g., the case $\vartheta = 3\pi/4$ produces the strongest signal and is most sensitive to axion masses around $m_\phi = 225$ eV. The probability ($\propto g_\phi^2$) to detect axions in this light-by-light scattering experiment is thus a hundred times that of PVLAS.

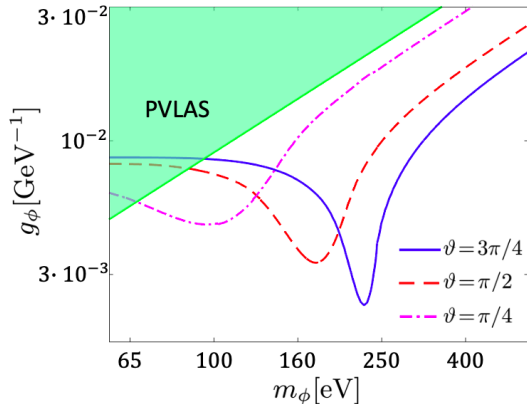


FIG. 4. Accessible parameter space based on $N_{\text{signal}} \geq 1$ from Eq. (7) in terms of axion mass m_ϕ and coupling g_ϕ . The optical laser orientations relative to the XFEL (at $\vartheta = 0$) are $\vartheta = 3\pi/4$ (blue solid curve), $\vartheta = \pi/2$ (red dashed curve) and $\vartheta = \pi/4$ (purple dot-dashed curve). The green shaded region in the top left corner denotes the parameter region probed by PVLAS.

Background Processes In view of the smallness of the signal, a discussion of its detectability should also include an estimate of possible background effects which might induce a false signal. These background effects are basically the same as already discussed in [70] devoted to the pure QED birefringence effect (see [72–95] and Appendix). Even without the optical laser, the nuclei could scatter x-ray photons via Thomson scattering, internal (nuclear) resonances, or Delbrück scattering, but these effects are too weak or do not generate a birefringent signal (to lowest order), see also [70]. As shown in the Appendix, including the pure QED vacuum birefringence effect does not alter our results significantly – at least near the axion resonance, which is the most important region here. Note that the pure QED vacuum birefringence effect would also yield a contribution without the Coulomb field of the nuclei (i.e., just from the optical laser, see, e.g., [72, 76–81]), but then the scattering angle would typically be much smaller (far below mrad).

Hence, presumably the most relevant background process is Compton or Thomson scattering from residual electrons. According to the particle-in-cell (PIC) simulations shown in [70], for example, there are $\mathcal{O}(10^4)$ electrons left in the interaction region. Inserting the differential cross section $d\sigma/d\Omega = \mathcal{O}(10^{-17} \mu\text{m}^2)$ for Thomson scattering and the solid angle of order $\mathcal{O}(10^{-5})$, we see that the scattering contributions from $\mathcal{O}(10^4)$ elec-

trons can be neglected if they add up incoherently. If the scattering amplitudes from these electrons would add up coherently, however, they could produce a detectable number of signal photons (within 10^3 shots with $\mathcal{O}(10^{12})$ XFEL photons each). Fortunately, the majority of these signal photons would have the same polarization as the incoming XFEL beam, i.e., they would not yield a birefringent signal. Birefringent Compton or Thomson scattering is further suppressed. For free electrons, it vanishes in forward direction as θ^4 , which would thus be negligible in our case. For electrons in the presence of a laser field, the suppression depends on the geometry [96]. If the magnetic field of the optical laser B_L is parallel to the XFEL propagation direction (Faraday case), as in the right plot in Fig. 3, the cross section for birefringent scattering is suppressed by an additional factor of $(qB_L/m\omega_{\text{in}})^2$, i.e., the square of the inverse combined Keldysh parameter [97, 98]. For our case, this gives an additional suppression by five orders of magnitude. If the magnetic field of the optical laser B_L is perpendicular to the XFEL propagation direction (Cotton-Mouton case), as in the left plot in Fig. 3, the suppression is even stronger [96]. As a consequence, the residual electrons do not pose a problem – unless there are too many of them.

Conclusions We have evaluated the axion contribution to birefringent light-by-light scattering for an XFEL probe and Coulomb-assisted optical laser pump. Special emphasis is placed on the resonant axion contribution which allows us to scan different axion masses by changing the involved parameters such as the angle ϑ between the XFEL and the optical laser. Furthermore, the axion resonance facilitates a sensitivity surpassing that of PVLAS, permitting the most stringent laboratory-based probe of virtual axion contributions.

Complementary to astrophysical bounds (e.g., [27]), such laboratory-based probes are also sensitive to axions which evade these bounds in some way. Examples could be interaction effects such as running coupling or confinement, see, e.g., [38, 39], which invalidate the picture of long-lived and free-streaming axions. Although we treated the axion field as a free massive scalar field for simplicity, our results can be generalized to this case by inserting the effective axion propagator into our amplitude. If this propagator displays one or more quasi-particle peaks, we would again obtain axion resonances. The width of these quasi-particle peaks (related to their life-time) would then be added to the width generated by the angular spread of the optical laser.

Outlook In order to advance the sensitivity further, one could use more intense optical lasers or XFELs or tighten the XFEL beam waist [71]. Another avenue is to explore different targets. For example, exploiting the recently observed phenomenon of relativistic transparency [99], one could envision a 10-40 nm thick foil or sheet which facilitates a much larger number of ionized nuclei in the optical laser focus.

* s.evans@hzdr.de

- [1] P. W. Higgs, Phys. Rev. Lett. **13** (1964), 508-509
- [2] R. D. Peccei and H. R. Quinn, Phys. Rev. Lett. **38** (1977), 1440-1443
- [3] S. Weinberg, Phys. Rev. Lett. **40** (1978), 223-226
- [4] F. Wilczek, Phys. Rev. Lett. **40** (1978), 279-282
- [5] J. E. Kim, Phys. Rev. Lett. **43** (1979), 103
- [6] M. A. Shifman, A. I. Vainshtein and V. I. Zakharov, Nucl. Phys. B **166** (1980), 493-506
- [7] A. R. Zhitnitsky, Sov. J. Nucl. Phys. **31** (1980), 260
- [8] M. Dine, W. Fischler and M. Srednicki, Phys. Lett. B **104** (1981), 199-202
- [9] J. Preskill, M. B. Wise and F. Wilczek, Phys. Lett. B **120** (1983), 127-132
- [10] P. Sikivie, Phys. Rev. Lett. **51** (1983), 1415-1417
- [11] G. G. Raffelt, 1996, ISBN 978-0-226-70272-8
- [12] G. G. Raffelt, Lect. Notes Phys. **741** (2008), 51-71
- [13] A. Ringwald, Phys. Dark Univ. **1** (2012), 116-135
- [14] J. L. Ouellet *et al.* Phys. Rev. Lett. **122** (2019) no.12, 121802
- [15] A. Caputo, M. Regis, M. Taoso and S. J. Witte, JCAP **03** (2019), 027
- [16] G. Alonso-Álvarez, R. S. Gupta, J. Jaeckel and M. Spannowsky, JCAP **03** (2020), 052
- [17] P. Carena, A. Mirizzi and G. Sigl, Phys. Rev. D **101** (2020) no.10, 103016
- [18] K. M. Backes *et al.* [HAYSTAC], Nature **590** (2021) no.7845, 238-242
- [19] J. Jaeckel and A. Ringwald, Ann. Rev. Nucl. Part. Sci. **60** (2010), 405-437
- [20] K. Baker *et al.* Annalen Phys. **525** (2013), A93-A99
- [21] A. Ayala, I. Domínguez, M. Giannotti, A. Mirizzi and O. Straniero, Phys. Rev. Lett. **113** (2014) no.19, 191302
- [22] I. G. Irastorza and J. Redondo, Prog. Part. Nucl. Phys. **102** (2018), 89-159
- [23] M. Buschmann, J. W. Foster and B. R. Safdi, Phys. Rev. Lett. **124** (2020) no.16, 161103
- [24] D. Cadamuro and J. Redondo, JCAP **02** (2012), 032
- [25] A. De Angelis, M. Roncadelli and O. Mansutti, Phys. Rev. D **76** (2007), 121301
- [26] J. F. Fortin, H. K. Guo, S. P. Harris, D. Kim, K. Sinha and C. Sun, Int. J. Mod. Phys. D **30** (2021) no.07, 2130002 doi:10.1142/S0218271821300020
- [27] A. Ringwald, L.J. Rosenberg and G. Rybka, "Axions and other similar particle," Chapter 90 in: R. L. Workman *et al.* [Particle Data Group], PTEP **2022** (2022), 083C01
- [28] J. Isern, E. Garcia-Berro, S. Torres and S. Catalan, Astrophys. J. Lett. **682** (2008), L109 doi:10.1086/591042
- [29] V. Anastassopoulos *et al.* [CAST], Nature Phys. **13** (2017), 584-590
- [30] M. Ahlers, H. Gies, J. Jaeckel and A. Ringwald, Phys. Rev. D **75** (2007), 035011
- [31] P. Brax, C. van de Bruck, A. C. Davis, D. F. Mota and D. J. Shaw, Phys. Rev. D **76** (2007), 124034
- [32] P. Brax, C. van de Bruck and A. C. Davis, Phys. Rev. Lett. **99** (2007), 121103
- [33] A. Dupays, E. Masso, J. Redondo and C. Rizzo, Phys. Rev. Lett. **98** (2007), 131802
- [34] H. Gies, J. Jaeckel and A. Ringwald, Phys. Rev. Lett. **97** (2006), 140402
- [35] J. Jaeckel, E. Masso, J. Redondo, A. Ringwald and F. Takahashi, Phys. Rev. D **75** (2007), 013004
- [36] Y. Liao, Phys. Lett. B **650** (2007), 257-261
- [37] R. N. Mohapatra and S. Nasri, Phys. Rev. Lett. **98** (2007), 050402
- [38] E. Masso and J. Redondo, JCAP **09** (2005), 015
- [39] E. Masso and J. Redondo, Phys. Rev. Lett. **97** (2006), 151802
- [40] G. Ruoso *et al.* Zeitschrift für Physik C Particles and Fields **56** (1992), 505-508
- [41] R. Cameron *et al.* Phys. Rev. D **47** (1993), 3707-3725
- [42] M. Fouche *et al.* Phys. Rev. D **78** (2008), 032013
- [43] P. Pagnat *et al.* [OSQAR], Phys. Rev. D **78** (2008), 092003
- [44] J. Redondo and A. Ringwald, Contemp. Phys. **52** (2011), 211-236
- [45] A. S. Chou *et al.* [GammeV (T-969)], Phys. Rev. Lett. **100** (2008), 080402
- [46] A. Afanasev, O. K. Baker, K. B. Beard, G. Biallas, J. Boyce, M. Minarni, R. Ramdon, M. Shinn and P. Slocum, Phys. Rev. Lett. **101** (2008), 120401
- [47] K. Ehret *et al.* Phys. Lett. B **689** (2010), 149-155
- [48] P. Pagnat *et al.* [OSQAR], Eur. Phys. J. C **74** (2014) no.8, 3027
- [49] R. Ballou *et al.* [OSQAR], Phys. Rev. D **92** (2015) no.9, 092002
- [50] T. Inada *et al.* Phys. Rev. Lett. **118** (2017) no.7, 071803
- [51] T. Yamaji, K. Tamasaku, T. Namba, T. Yamazaki and Y. Seino, Phys. Lett. B **782** (2018), 523-527
- [52] L. Maiani, R. Petronzio and E. Zavattini, Phys. Lett. B **175** (1986) 359.
- [53] G. Raffelt and L. Stodolsky, Phys. Rev. D **37** (1988), 1237
- [54] D. Bernard, Nuovo Cim. A **110** (1997), 1339-1346
- [55] S. Villalba-Chavez and A. Piazza, JHEP **11** (2013), 136
- [56] D. Tommasini, A. Ferrando, H. Michinel and M. Seco, JHEP **11** (2009), 043
- [57] B. Dobrich and H. Gies, JHEP **10** (2010), 022
- [58] S. Evans and J. Rafelski, Phys. Lett. B **791** (2019), 331-334
- [59] Z. Bogorad, A. Hook, Y. Kahn and Y. Soreq, Phys. Rev. Lett. **123** (2019) no.2, 021801
- [60] S. Shakeri, D. J. E. Marsh and S. S. Xue, [arXiv:2002.06123 [hep-ph]].
- [61] K. A. Beyer, G. Marocco, C. Danson, R. Bingham and G. Gregori, Phys. Lett. B **839** (2023), 137759
- [62] K. Homma *et al.* [SAPPHIRES], JHEP **12** (2021), 108
- [63] F. Ishibashi, T. Hasada, K. Homma, Y. Kirita, T. Kanai, S. Masuno, S. Tokita and M. Hashida, Universe **9** (2023) no.3, 123
- [64] E. Zavattini *et al.* [PVLAS], Phys. Rev. Lett. **96** (2006), 110406
- [65] E. Zavattini *et al.* [PVLAS], Phys. Rev. D **77** (2008), 032006
- [66] A. Ejlli, F. Della Valle, U. Gastaldi, G. Messineo, R. Pengo, G. Ruoso and G. Zavattini, Phys. Rept. **871** (2020), 1-74
- [67] R. Battesti, *et al.* Eur. Phys. J. D **46** (2008) 323-333
- [68] R. Battesti *et al.* Phys. Rept. **765-766** (2018), 1-39
- [69] X. Fan *et al.* Eur. Phys. J. D **71** (2017) no.11, 308
- [70] N. Ahmadinia, M. Busmann, T. E. Cowan, A. Debus, T. Kluge and R. Schützhold, Phys. Rev. D **104** (2021) no.1, L011902

- [71] U. Zastra *et al.* J. Synchrotron Rad. (2021). **28**, 1393–1416
- [72] N. Ahmadinia, T. E. Cowan, J. Grenzer, S. Franchino-Viñas, A. L. Garcia, M. Šmíd, T. Toncian, M. A. Trejo and R. Schützhold, [arXiv:2208.14215 [physics.optics]].
- [73] W. Heisenberg and H. Euler, *Z. Phys.* **98**, 714 (1936).
- [74] V. Weisskopf, Kong. Dan. Vid. Sel. Mat. Fys. Med. **14**, N6, 1 (1936).
- [75] J. S. Schwinger, *Phys. Rev.* **82**, 664 (1951).
- [76] A. Di Piazza, K. Z. Hatsagortsyan and C. H. Keitel, *Phys. Rev. Lett.* **97** (2006), 083603
- [77] T. Heinzl, B. Liesfeld, K. U. Amthor, H. Schwöerer, R. Sauerbrey and A. Wipf, *Opt. Commun.* **267** (2006), 318-321
- [78] H. P. Schlenvoigt, T. Heinzl, U. Schramm, T. E. Cowan and R. Sauerbrey, *Phys. Scripta* **91** (2016) no.2, 023010
- [79] T. Inada, T. Yamazaki, T. Yamaji, Y. Seino, X. Fan, S. Kamioka, T. Namba and S. Asai, *Science* **7** (2017), 671
- [80] Y. Seino, T. Inada, T. Yamazaki, T. Namba and S. Asai, *PTEP* **2020** (2020) no.7, 073C02
- [81] F. Karbstein, D. Ullmann, E. A. Mosman and M. Zepf, *Phys. Rev. Lett.* **129** (2022) no.6, 061802
- [82] T. Inada *et al.* *Phys. Lett. B* **732** (2014), 356-359
- [83] E. Lundstrom, G. Brodin, J. Lundin, M. Marklund, R. Bingham, J. Collier, J. T. Mendonca and P. Norreys, *Phys. Rev. Lett.* **96** (2006), 083602
- [84] A. Di Piazza, A. I. Milstein and C. H. Keitel, *Phys. Rev. A* **76** (2007), 032103
- [85] B. King, H. Hu and B. Shen, *Phys. Rev. A* **98** (2018) no.2, 023817
- [86] D. Tommasini and H. Michinel, *Phys. Rev. A* **82** (2010), 011803
- [87] B. King and C. H. Keitel, *New J. Phys.* **14** (2012), 103002
- [88] H. Gies, F. Karbstein, C. Kohlfürst and N. Seegert, *Phys. Rev. D* **97** (2018) no.7, 076002
- [89] H. Gies, F. Karbstein and C. Kohlfürst, *Phys. Rev. D* **97** (2018) no.3, 036022
- [90] B. Dobrich and H. Gies, *EPL* **87** (2009) no.2, 21002
- [91] H. Gies, F. Karbstein and N. Seegert, *New J. Phys.* **17** (2015) no.4, 043060
- [92] H. Grote, *Phys. Rev. D* **91** (2015) no.2, 022002
- [93] S. Robertson *et al.*, *Phys. Rev. A* **103** (2021) no.2, 023524
- [94] H. Gies, F. Karbstein and L. Klar, *Phys. Rev. D* **106** (2022) no.11, 116005
- [95] F. Karbstein, C. Sundqvist, K. S. Schulze, I. Uschmann, H. Gies and G. G. Paulus, *New J. Phys.* **23** (2021) no.9, 095001
- [96] N. Ahmadinia, T. E. Cowan, M. Ding, M. A. L. Lopez, R. Sauerbrey, R. Shaisultanov and R. Schützhold, [arXiv:2212.03350 [hep-ph]].
- [97] R. Schützhold, H. Gies and G. Dunne, *Phys. Rev. Lett.* **101** (2008), 130404
- [98] G. Torgrimsson, C. Schneider and R. Schützhold, *Phys. Rev. D* **97** (2018) no.9, 096004
- [99] P. L. Poole *et al.* *New J. Phys.* (2018) **20**, 013019

Axion s-channel amplitude We compute the s-channel amplitude (first diagram in Fig. 5)

$$\mathfrak{A}_{\pm}^s = \mathfrak{A}_{\text{CL}\pm}^s + \mathfrak{A}_{\text{LC}\pm}^s, \quad (8)$$

including both cases of absorbed and emitted optical photons, labelled with subscripts \pm . ‘CL’ labels the sequence

where the axion is generated by the XFEL-Coulomb field collision followed by conversion back into an XFEL photon via coupling to the optical laser, and ‘LC’ the opposite sequence. We present the more involved CL case in detail, which simplifies in the LC case.

Expressed as integrals over the optical laser momentum transfer k_L ,

$$\begin{aligned} \mathfrak{A}_{\text{CL}\pm}^s &= -ig_\phi^2 \int \frac{d^3 k_L}{(2\pi)^3} \frac{k_{\text{in}}^\alpha \epsilon_{\text{in}}^{\beta*} \epsilon_{\mu\nu\alpha\beta} k_C^\mu \underline{A}_C^\nu(k_C)}{(k_{\text{out}} \mp q)^2 - m_\phi^2} \\ &\quad \times k_{\text{out}}^\alpha \epsilon_{\text{out}}^\beta \epsilon_{\mu\nu\alpha\beta} k_L^\mu \underline{A}_L^\nu(k_L), \\ \mathfrak{A}_{\text{LC}\pm}^s &= \mathfrak{A}_{\text{CL}\pm}^s(k_{\text{out}} \leftrightarrow -k_{\text{in}}, \epsilon_{\text{out}} \leftrightarrow \epsilon_{\text{in}}). \end{aligned} \quad (9)$$

The energy-momentum conservation (see (2)) is, in more general form including both emitted and absorbed optical photon cases,

$$\omega_{\text{out}} = \omega_{\text{in}} \pm \omega_L, \quad \mathbf{k}_{\text{out}} = \mathbf{k}_{\text{in}} \pm \mathbf{k}_L + \mathbf{k}_C. \quad (10)$$

Applying the Coulomb potential (4) and the optical laser using a Gaussian distribution function, the products with the Levi-Civita tensors in (9) are given by

$$\begin{aligned} k_{\text{in}}^\alpha \epsilon_{\text{in}}^{\beta*} \epsilon_{\mu 0 \alpha \beta} k_C^\mu \underline{A}_C^0(k_C) &= -2\pi \frac{Q\delta(k_C^0)}{\mathbf{k}_C^2} \mathbf{e}_{\text{in}}^* \cdot (\mathbf{k}_C \times \mathbf{k}_{\text{in}}), \\ k_{\text{out}}^\alpha \epsilon_{\text{out}}^\beta \epsilon_{\mu\nu\alpha\beta} k_L^\mu \underline{A}_L^\nu(k_L) &= (2\pi)^2 \delta(\omega_L - |\mathbf{k}_L|) \frac{|\mathbf{E}|}{\omega_L} \\ &\quad \times \frac{e^{-(1-\mathbf{n}_L \cdot \mathbf{N}_L)\omega_L^2/w_\perp^2}}{w_\perp^2} \mathbf{e}_{\text{out}} \cdot ((\omega_{\text{out}} \mathbf{k}_L - \omega_L \mathbf{k}_{\text{out}}) \times \mathbf{e}_L), \end{aligned} \quad (11)$$

including $2\pi\delta(k_C^0) = 2\pi\delta(\omega_{\text{out}} \mp \omega_L - \omega_{\text{in}})$ to account for the time-independence of the Coulomb field. \mathbf{N}_L labels the propagation direction of the optical laser pulse, and width $w_\perp = \omega_L/6$ gives the transverse momentum spread. From (11), a general expression for any XFEL and optical laser configuration, we recover the special case in (5) by taking $\text{CL} \rightarrow \text{LC}$, and the fully perpendicular case $\mathbf{n}_L \parallel \mathbf{e}_{\text{out}}$ and $\mathbf{e}_L \parallel \mathbf{n}_{\text{in}}$.

We plug (11) into the amplitude (9) and integrate $|\mathbf{k}_L|$ to get

$$\begin{aligned} \mathfrak{A}_{\text{CL}\pm}^s &= i \frac{g_\phi^2 Q |\mathbf{E}| \omega_{\text{in}} \omega_{\text{out}} \omega_L^2}{w_\perp^2} \delta(\omega_{\text{out}} \mp \omega_L - \omega_{\text{in}}) \\ &\quad \times \int d\Omega_L \frac{e^{-(1-\mathbf{n}_L \cdot \mathbf{N}_L)\omega_L^2/w_\perp^2}}{\mathbf{k}_C^2} \\ &\quad \times \frac{\mathbf{e}_{\text{in}}^* \cdot (\mathbf{k}_C \times \mathbf{n}_{\text{in}}) \mathbf{e}_{\text{out}} \cdot ((\mathbf{n}_L - \mathbf{n}_{\text{out}}) \times \mathbf{e}_L)}{\mp 2\omega_{\text{out}} \omega_L (1 - \mathbf{n}_L \cdot \mathbf{n}_{\text{out}}) - m_\phi^2}, \end{aligned} \quad (12)$$

with resonant contributions for the axion mass range

$$m_\phi < \sqrt{4\omega_{\text{out}} \omega_L}. \quad (13)$$

At larger masses outside this range, the off-resonance amplitude can be immediately carried out numerically and applied to compute the cross section (6).

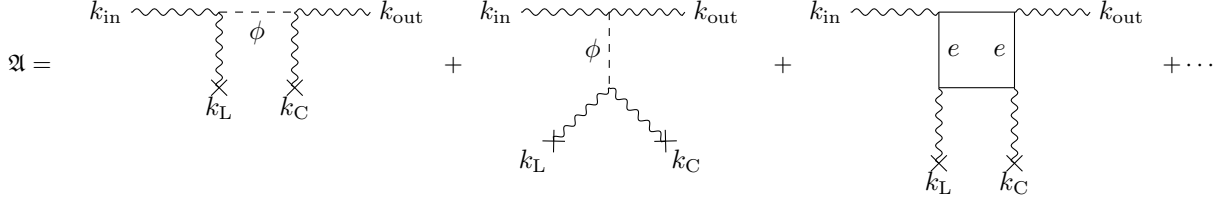


FIG. 5. Axion s and t -channels and QED box diagram for Coulomb-assisted light-light scattering.

For the range of axion masses (13), further steps can simplify the numerical evaluation. We choose coordinates such that the scattered photon \mathbf{n}_{out} points along $\theta_L = 0$, so that the pole in (12) depends only one coordinate: $\mathbf{n}_L \cdot \mathbf{n}_{\text{out}} = \cos(\theta_L)$. The resonance is located at

$$\theta_L = \theta_{\text{res}} \equiv \arccos\left(1 - \frac{m_\phi^2}{2\omega_{\text{out}}\omega_L}\right). \quad (14)$$

Shifting the integration over θ_L as $\theta_L \rightarrow \theta_{\text{res}} + \theta_L$, and expanding the denominator in the last line of (12) in powers of θ_L ,

$$\begin{aligned} & \frac{1}{2\omega_{\text{out}}\omega_L(1 - \cos(\theta_{\text{res}} + \theta_L)) - m_\phi^2 + im_\phi\Gamma} \\ &= \frac{1}{2\omega_{\text{out}}\omega_L \sin(\theta_{\text{res}})} \frac{1}{\theta_L + i \frac{m_\phi\Gamma}{2\omega_{\text{out}}\omega_L \sin(\theta_{\text{res}})}}. \end{aligned} \quad (15)$$

We plug (15) into (12) and integrate θ_L using the relation $\int dx f(x)/(x + i\Gamma) = -i\pi f(-i\Gamma) + \text{P} \int dx f(x - i\Gamma)/x$.

The same procedure follows for computing the amplitude for the reverse sequence $\mathfrak{A}_{\text{LC}\pm}^s$. Aside from the replacement $\mathbf{k}_{\text{out}} \leftrightarrow -\mathbf{k}_{\text{in}}$, $\mathbf{e}_{\text{out}} \leftrightarrow \mathbf{e}_{\text{in}}$, we integrate over $d\Omega_q$ with \mathbf{n}_{in} pointing along $\theta_L = 0$ instead, which is simpler to implement numerically.

Axion t -channel amplitude We compute the t -channel amplitude described by the second diagram in Fig. 1. The amplitude

$$\begin{aligned} \mathfrak{A}_{\pm}^t &= -ig_\phi^2 \int \frac{d^3k_L}{(2\pi)^3} \frac{\underline{k}_{\text{in}}^\alpha \underline{e}_{\text{in}}^{\beta*} \epsilon_{\mu\nu\alpha\beta} \underline{k}_{\text{out}}^\mu \underline{e}_{\text{out}}^\nu}{(\underline{k}_{\text{out}} - \underline{k}_{\text{in}})^2 - m_\phi^2} \\ &\quad \times \underline{k}_{\text{C}}^\alpha \underline{A}_{\text{C}}^\beta(k_{\text{C}}) \epsilon_{\mu\nu\alpha\beta} \underline{k}_{\text{L}}^\mu \underline{A}_{\text{L}}^\nu(k_{\text{L}}), \end{aligned} \quad (16)$$

with \underline{k}_{C} following (2). The products with the Levi-Civita tensors

$$\begin{aligned} \underline{k}_{\text{in}}^\alpha \underline{e}_{\text{in}}^{\beta*} \epsilon_{\mu\nu\alpha\beta} \underline{k}_{\text{out}}^\mu \underline{e}_{\text{out}}^\nu &= \mathbf{e}_{\text{in}} \cdot ((\omega_{\text{in}}\mathbf{k}_{\text{out}} - \omega_{\text{out}}\mathbf{k}_{\text{in}}) \times \mathbf{e}_{\text{out}}), \\ \underline{k}_{\text{C}}^\alpha \underline{A}_{\text{C}}^\beta(k_{\text{C}}) \epsilon_{\mu\nu\alpha\beta} \underline{k}_{\text{L}}^\mu \underline{A}_{\text{L}}^\nu(k_{\text{L}}) &= -(2\pi)^3 \delta(\omega_L - |\mathbf{k}_L|) \\ &\quad \times \frac{Q\delta(\underline{k}_{\text{C}}^0)}{\mathbf{k}_{\text{C}}^2} \frac{|\mathbf{E}|}{\omega_L} \frac{e^{-(1-\mathbf{n}_L \cdot \mathbf{N}_L)\omega_L^2/w_\perp^2}}{w_\perp^2} \mathbf{e}_L \cdot (\mathbf{k}_{\text{C}} \times \mathbf{k}_L). \end{aligned} \quad (17)$$

Carrying out the integration, the same steps as in the s -channel case follow.

We note that the amplitude (16) gives exclusively off-resonant contributions: the scalar propagator denominator is $-2\omega_{\text{out}}\omega_{\text{in}}(1 - \mathbf{n}_{\text{out}} \cdot \mathbf{n}_{\text{in}}) - m_\phi^2$. All terms are the same sign for both cases where the optical photon is absorbed and emitted.

QED amplitude We evaluate the QED amplitude, the third diagram in Fig. 1. The standard procedure of computing the Feynman diagram would be more challenging than the tree-level axion contribution, due to the spatial dependence of Coulomb field being sharply varying on the electron Compton wavelength scale.

A simplified approach comes from considering how energy-momentum conservation governs the possible momentum transfer from the Coulomb field, entering through one of the four external photon lines. The XFEL and optical laser external photon lines restrict the possible Coulomb momentum transfer to order eV, many orders of magnitude below the electron mass scale. In addition to energy-momentum conservation restrictions, only within the deflection angle $\theta < 2\text{mrad}$ (eV momentum transfer) is the signal coherent. Thus while the combined probe and pump fields are sharply varying in time and space as seen by the $\sim 100\text{eV}$ axion, they are smooth for the (511keV) electron.

We consider exclusively the pseudoscalar $\mathbf{B} \cdot \mathbf{E}$ -dependent light-light scattering contributions, so that the effective Lagrangian

$$\mathcal{L} = \frac{\mathbf{E}^2 - \mathbf{B}^2}{2} + \mathcal{L}_{\text{QED}} + \mathcal{L}_\phi, \quad (18)$$

with the Maxwell contribution followed by QED and axion interactions to light-light scattering order. The pseudoscalar ($\mathbf{B} \cdot \mathbf{E}$ -dependent) QED e^+e^- contribution [73–75] and the axion contribution \mathcal{L}_ϕ in the heavy mass limit (quasi-constant field $\omega \ll m_\phi$) [52, 54, 58]

$$\mathcal{L}_{\text{QED}} = \frac{14\alpha^2}{45m_e^4} (\mathbf{B} \cdot \mathbf{E})^2, \quad \mathcal{L}_\phi^{\omega \ll m_\phi} = \frac{g_\phi^2}{2m_\phi^2} (\mathbf{B} \cdot \mathbf{E})^2, \quad (19)$$

where $\alpha = e^2/4\pi = 1/137$ and m_e is the electron mass. Taking the ratio of the two contributions,

$$\frac{\mathcal{L}_{\text{QED}}}{\mathcal{L}_\phi^{\omega \ll m_\phi}} = \frac{28\alpha^2 m_\phi^2}{45m_e^4 g_\phi^2}. \quad (20)$$

We obtain the QED amplitude by multiplying the ALP amplitudes by the ratio (20) and taking the heavy axion mass limit:

$$\mathfrak{A}_{\pm}^{\text{QED}} = \frac{28\alpha^2}{45m_e^4} \frac{m_\phi^2}{g_\phi^2} \lim_{\omega/m_\phi \rightarrow 0} (\mathfrak{A}_{\pm}^s + \mathfrak{A}_{\pm}^t), \quad (21)$$

for comparison see (9) of [70], using a constant magnetic field in place of the optical laser.

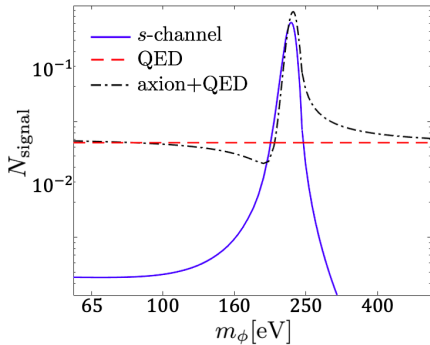


FIG. 6. Number of scattered photons N_{signal} in (7), as a function of m_ϕ , at fixed coupling $g_\phi = 2.5 \cdot 10^{-3} \text{GeV}^{-1}$. Plots show the axion s -channel contribution (blue, solid), the combined effect of axion s and t -channels, QED, and their interference (black, dot-dashed), and exclusively QED (red, dashed). For all plots the optical laser configuration is: $\vartheta = 3\pi/4$, with polarization $\mathbf{e}_L \cdot \mathbf{e}_{\text{in}} = 0$.

Axion-QED interference effects It is important to note that the main result in this work is based on the resonant axion interaction, where the s -channel axion contribution dominates. At lighter or heavier axion masses, off of the resonant peaks in Fig. 4, QED and axion-QED interference effects become important. To quantify such effects we apply the QED result (21) alongside both the s (12) and t -channel (16) axion amplitudes to compute the cross section for all diagrams. We plot the deflected photons per XFEL shot in Fig. 6 comparing the dominant at resonance s -channel to the total signal considering all diagrams and their interference.

As expected at resonance, the axion s -channel diagram (blue, solid) dominates, with a signal an order of magnitude stronger than the QED effect. Slightly off the resonance, the total axion and QED contribution (black, dot-dashed) exhibits constructive interference at heavier masses above resonance and destructive interference at lighter masses, due to the sign flip in the axion propagator. Far from resonance, the purely QED contribution (red, dashed) dominates.